Phys. Status Solidi B **253,** No. 8, 1529–1536 (2016) / **DOI** 10.1002/pssb.201552680

physica status solidi b
www.pss-b.com
basic solid state physics

Neutron diffraction study of microstructural and magnetic effects in fine particle NiO powders

A. M. Balagurov[1], I. A. Bobrikov[*,1], S. V. Sumnikov[1], V. Yu. Yushankhai[2], J. Grabis[3], A. Kuzmin[4], N. Mironova-Ulmane[4], and I. Sildos[5]

[1] Frank Laboratory of Neutron Physics, Joint Institute for Nuclear Research, RU-141980 Dubna, Russian Federation
[2] Bogoliubov Laboratory of Theoretical Physics, Joint Institute for Nuclear Research, RU-141980 Dubna, Russian Federation
[3] Institute of Inorganic Chemistry, Riga Technical University, Miera Street 34, LV-2169 Salaspils, Latvia
[4] Institute of Solid State Physics, University of Latvia, Kengaraga Street 8, LV-1063 Riga, Latvia
[5] Institute of Physics, University of Tartu, Ravila 14c, 50411 Tartu, Estonia

Received 24 October 2015, revised 17 February 2016, accepted 25 February 2016
Published online 21 March 2016

Keywords core–shell model, crystal structure, magnetic structure, neutron diffraction, NiO, submicron particles

[*] Corresponding author: e-mail bobrikov@nf.jinr.ru, Phone: +7-49621-66580, Fax: +7-49621-65484
URL: http://www.jinr.ru/ (I. A. Bobrikov)

Nickel oxide powders with grain sizes ranging from 100 to 1500 nm have been studied by high-resolution neutron diffraction. We have found that the atomic structure, the antiferromagnetic ordering, and the value of the nickel magnetic moments inherent in the bulk material of NiO are still preserved and are nearly independent of the average size of the grains. The sizes of the coherently scattering atomic and magnetic domains were estimated independently owing to a complete separation of the nuclear and magnetic peaks in the neutron diffraction patterns. It is shown that the finite-size and surface disorder effects in particles at the submicron scale have a more pronounced influence on the magnetism than on their structural properties. We conclude that the core–shell model suggested earlier for nanosized particles can be successfully extended to particles whose sizes are in the submicron range.

1 Introduction The design of magnets for small-scale applications requires understanding, in particular, how the structural and magnetic properties of fine particles evolve as their size reduces from the micrometer to the nanometer scale. In this respect, the influence of finite-size and surface effects on the magnetic behavior of fine particles is being actively studied by various physical methods with the main focus on the specific magnetic properties that are markedly different from those in the parent ferro- or antiferromagnetic bulk materials. A large number of papers and reviews (see, e.g., Refs. [1–7]) are devoted to the discussion of the properties of nanosized particles, including numerous methods of their production, experimental measurements, and theoretical concepts used.

As is known [8–10], the behavior of an individual fine particle, with the intrinsic ferromagnetic (FM) or antiferromagnetic (AFM) interaction, is dictated not only by its characteristic size and shape, but also by microstructural features influencing the mechanisms of the spin interactions. Microstructural surface effects that are due to broken lattice bonds (and defects) result in variations in the number of atomic neighbors and interatomic distance not only for the surface atoms, but frequently in the next submerged layers [11]. The surface disorder and roughness influence the spin exchange coupling and produce a generally site-dependent spin anisotropy, thus promoting, in the near-surface region, a kind of spin disorder as well.

The finite-size effects are usually understood as those originating from the cut off of some characteristic length due to the purely geometrical constraint of finite volume. The principal effect on a magnetic particle of this finite size is the breaking of a large number of exchange bonds for the under-coordinated surface atoms. The importance of the surface and finite-size effects, which have a particularly profound impact on AFM materials like nickel oxide, NiO, increases inversely with the particle size [12–14]. However,

both kinds of effects are mixed and in competition, which makes it difficult to observe their tracks separately [1].

Most of the observed properties of nanosized NiO particles can be explained, at least qualitatively, in terms of the core–shell model [15]. The experimental data obtained in numerous measurements [16, 17, 18, 19, 20] including temperature and field dependent magnetization, *ac* and *dc* susceptibilities, together with methods of structural characterization, indicate that the particle magnetization is not uniform. It can be considered as consisting of an AFM ordered core (probably, with a comparatively small uncompensated magnetic moment due to mutual sublattices canting) and a magnetically and structurally disordered outer shell (whose frozen magnetic moment at low temperatures may reach a large value) with the core–shell interface exchange coupling that strongly influences the overall magnetic behavior of a particle.

Complementary to the methods of X-ray diffraction and absorption spectroscopy, transmission electron microscopy (TEM), and high-resolution TEM (widely used to measure the fine-particle internal structure) there is also neutron diffraction, which has the great advantage that, for instance, in simple oxides, like NiO with AFM structure, nuclear and magnetic diffraction peaks are well separated and, hence, their characteristics can be analyzed independently. This means that neutron diffraction allows measuring simultaneously a degree of lattice order (the characteristic size of the coherently scattering domains) and the related magnetic order. The results of the experimental study in this direction of a polydisperse nanopowder NiO were reported recently in Ref. [20]. The length of the coherently scattering AFM domains was estimated to be smaller than the mean size of the crystallites, thus showing the existence of the magnetically disordered outer layer and supporting the validity of the core–shell model for NiO nanoparticles. Assuming spherical particle shape, the authors obtained 6.5 and 5.1 nm for "crystal" and "magnetic" particle diameters, respectively, thus showing the existence of the magnetically disordered outer layer and supporting the validity of the core–shell model for NiO nanoparticles. We note also an earlier neutron diffraction study [21], where qualitatively similar results were reported for NiO nanoparticles having a highly anisotropic shape.

In Ref. [22], three NiO powder samples with average grain sizes of $\langle D\rangle = 13$, 100, and 1500 nm were studied by several methods, including neutron diffraction, SQUID magnetometry, and Raman spectroscopy. The existence of conventional AFM ordering and the absence of any noticeable distortions of the crystal structure in comparison with the bulk samples was confirmed, but the low resolution of the neutron diffractometer did not allow obtaining direct data on the sizes of the coherently scattering atomic (structural) and magnetic domains.

As a continuation of these studies, we have performed additional high-resolution neutron diffraction measurements for a set of fine particle NiO powders with mean grain sizes ranging from 100 to 1500 nm (preliminary results were reported briefly in the conference article [23]). In the present study, a procedure is developed and aimed at revealing a relation between the long-range crystalline and magnetic orders observed by means of high-resolution neutron diffraction in NiO fine particles of different sizes. The procedure is shown to be especially efficient for particles of submicron size, and we suggest that the validity of the core–shell model for NiO can be extended from the nanometer to the submicron scale.

2 Experimental Three NiO powders (S1, S2, and S3 hereafter) were produced by the evaporation of the coarse grained commercially available NiO (99.9%) powder in the radio-frequency plasma as described in Ref. [24]. The synthesis was performed using a flow rate of plasma forming gas of $8.0\,m^3\,h^{-1}$, a raw feeding rate of $0.6–1.2\,kg\,h^{-1}$, and a flow rate of cooling gas of $0.6–50\,m^3\,h^{-1}$. The cooling gas was introduced into the vapor region of the nickel oxide to control the growth of the particles, and two powders with specific surface areas equal to 9.0 and $6.4\,m^2\,g^{-1}$ were produced. These two powders (samples S2 and S3, both with a light green color) were used as-prepared. Sample S3 with dark green color was produced from sample S2 by annealing in air at 1000 °C, so its specific surface area was reduced from 6.4 to $0.6\,m^2\,g^{-1}$.

The average particle sizes of the prepared NiO samples (S1–S3) were estimated from the specific surface areas, calculated from the nitrogen gas adsorption–desorption isotherms (the Brunauer–Emmett–Teller (BET) method), determined at 77 K using a Kelvin Sorptometer 1042 (Costech Int.): they are 100 (S1), 138 (S2), and 1500 nm (S3). Realistic uncertainties of this method can hardly be determined. An experience shows that for particles of about 150 nm, the uncertainty is close to 5%, i.e., ~7 nm. We believe that the size of the particles obtained by this method should be considered as reference one. Hereafter it is marked as $\langle D\rangle$. It is worth mentioning that the methods used for the preparation of powders at the submicron scale, lead to crystallite size distribution with dispersity of about 10 nm.

The neutron diffraction patterns were measured at two temperatures: 5 and 293 K, with a high resolution Fourier diffractometer (HRFD) [25], at the IBR-2 pulsed reactor in JINR (Dubna). An HRFD is a time-of-flight (TOF) diffractometer with a correlation mode of data acquisition. Its $\Delta d/d$ resolution is determined by the maximum frequency of the fast Fourier chopper. In routine operation ($V_{max} = 4000$ rpm), $\Delta d/d \approx 0.001$ for $d = 2$ Å only slightly depends on d_{hkl}, and improves with increasing d_{hkl}. It is worth noting that the previous practice in studies of the microstructural effects at HRFD showed that microstresses in crystallites present at the level of $\varepsilon = 0.0003$ or more, as well as the average sizes of coherently scattering domains at the level of $L_{coh} = 350$ nm or less, can be detected with the required accuracy. In parallel with gathering the high-resolution diffraction patterns at HRFD conventional TOF-patterns (without the use of correlation analysis) with an average resolution (of $\Delta d/d \approx 0.01–0.02$) were also

measured. For a precise determination of the HRFD resolution functioning, Al_2O_3, $^{11}LaB_6$ (both from the NIST standards series) and $Na_2Al_2Ca_3F_{14}$ (NAC) powders were used.

The HRFD design allows us to measure diffraction patterns in high resolution mode with two back-scattering ($2\theta = \pm 152^\circ$) detectors for d_{hkl} in a range of 0.6–3.6 Å and with the $2\theta = 90^\circ$ detector in the 0.8–4.9 Å range. With the same detectors in the average resolution mode, diffraction patterns can be registered up to 4.5 and 6.0 Å, respectively.

The diffraction patterns of all the NiO samples measured by all the detectors were found to be of good quality with no impurity phases revealed (Fig. 1). In this figure (as well as in some others) the diffraction pattern is corrected (normalized) for the intensity distribution in the incident neutron beam, as it is usually used for presentation of scattering spectra measured with TOF diffractometers. No perceptible changes in the diffraction peak intensities or the background levels were observed at temperatures down to 5 K.

In the paper of Cooper et al. [20] already cited above a nanoparticle sample of NiO was studied and, by reason of experimental limitations inherent to the technique used in this study, the only one magnetic and one nuclear diffraction lines were analyzed using the Scherrer equation. In contrast, our technique allows to determine the characteristics of many nuclear and several magnetic diffraction lines with the use of more advanced and adequate Rietveld and Williamson-Hall methods for their analysis.

3 Results The lattice of bulk NiO in the paramagnetic phase ($T > T_N = 523$ K) has cubic symmetry (space group $Fm\bar{3}m$, $a_C \approx 4.175$ Å) and a simple NaCl-type structure.

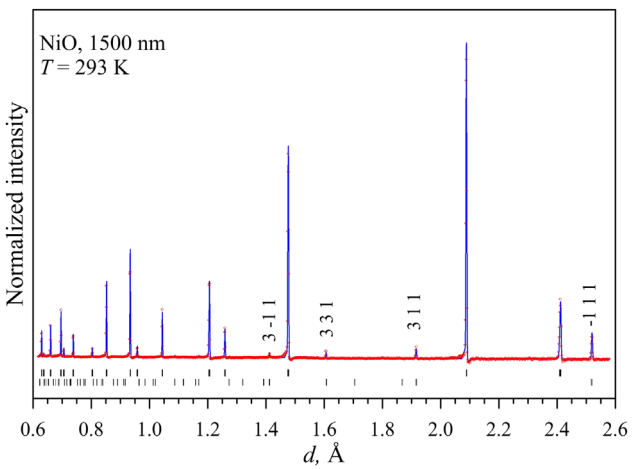

Figure 1 An example of the neutron diffraction pattern of the S3 (1500 nm) sample measured at room temperature. Vertical bars indicate peak positions (from top to bottom) of crystal and magnetic phases. The Miller indices of several magnetic peaks are indicated (indices of doubled R-unit cell). A slight asymmetry of peaks profiles is connected with special features of the correlation mode of data acquisition at HRFD.

Below the Néel temperature, the lattice acquires a rhombohedral distortion (space group $R\bar{3}m$, $a_R = a_C/\sqrt{2} = 2.952$ Å, $\alpha = 60.07^\circ$), which increases as the temperature decreases. The visible deviation from cubic metrics and the related splitting of the diffraction peaks are so small that for them to be revealed by neutron scattering requires high resolution diffractometers. How the rhombohedral distortion is revealed in the diffraction peak profile, measured with HRFD at low temperature, is shown in Fig. 2.

At room and lower temperatures, the magnetic moments of Ni were confirmed to be ordered with the propagation vector $\mathbf{k} = [1/2\ 1/2\ 1/2]$ in the cubic cell, which is identical to $\mathbf{k} = [0\ 0\ 3/2]$ in the hexagonal cell associated with the rhombohedral cell. This means that the moments aligned ferromagnetically in the {111} planes are staggered in a direction perpendicular to these planes. Thus, the linear parameters of the rhombohedral magnetic cell are doubled compared to the nuclear one, $a_{mag} = 2a_R = 5.904$ Å, whereas the angle parameter does not change, $\alpha = 60.07^\circ$ (doubled R-unit cell). The maximum d_{hkl} in this cell is about 4.82 Å, which is well observed in the neutron diffraction patterns measured in the average resolution mode (Fig. 3).

For diffraction data processing, the Rietveld method was used so as to refine the structural and magnetic parameters, together with the analysis of the separate diffraction peak profiles to determine their widths.

3.1 Rietveld refinement The analysis of the diffraction patterns by the Rietveld method was carried out using the MRIA [26] and FullProf [27] packages. The MRIA program has been written specially for analysis of data obtained with HRFD instrument having nonstandard profile of diffraction lines and we used it for structural analysis. FullProf was used for refinement of NiO magnetic moments. The analysis was performed in the two-phase option in the 0.6–2.6 Å d-range (Fig. 4), the widths of the nuclear and magnetic diffraction peaks were refined

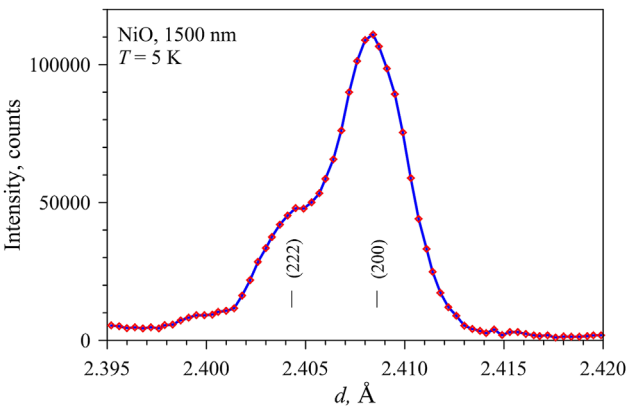

Figure 2 Splitting of (200) and (222) diffraction lines (indices of doubled R-unit cell) owing to lattice rhombohedral distortion ($\alpha = 60.09^\circ$), measured with the S3 sample at low temperature. The relative d-spacings difference is about 0.00145.

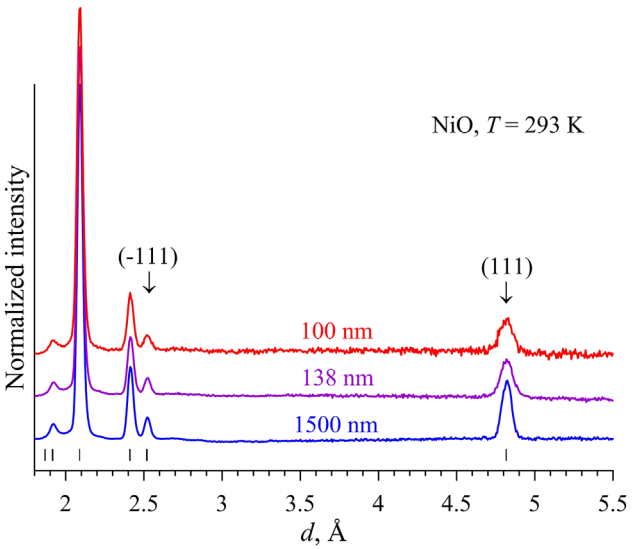

Figure 3 Diffraction patterns of all S1–S3 samples measured in the average resolution mode at room temperature in the large d-spacings range. Vertical bars are calculated peak positions. The Miller indices of doubled R-unit cell for two first magnetic peaks are pointed. Diffraction intensities are only slightly changed under temperature lowering to 5 K.

independently. The convergence of the minimization process for all high-resolution diffraction patterns was satisfactory.

The results of data processing are summarized in Table 1. From these data one can see that as the grain mean size decreases, the unit cell remains almost invariable. In the MRIA program it is possible to refine parameters, the combination of which allows to characterize (in some arbitrary units) the average width of the nuclear and magnetic peaks in the diffraction spectrum. In Table 1 these values are marked as $\langle W \rangle_{nuc}$ and $\langle W \rangle_{mag}$. In Fig. 5 they

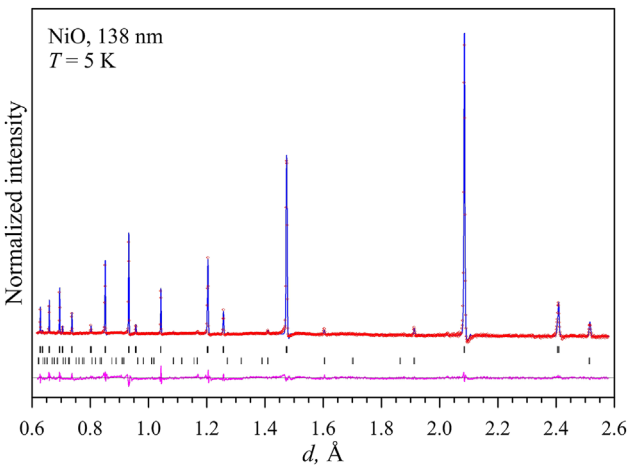

Figure 4 Example of the Rietveld refinement patterns and difference plots (in the bottom) of the S2 (138 nm) sample measured at low temperature. Vertical bars indicate peak positions (from top to bottom) of crystal and magnetic phases.

are shown for samples S1, S2, S3 as a function of crystallites size, estimated by BET method. Obviously size reducing leads to a sharp increase in the width of both nuclear and magnetic peaks. Moreover, if for S3 ($\langle D \rangle = 1500$ nm), $\langle W \rangle_{mag} \approx \langle W \rangle_{nuc}$ (within errors limit), for S2 ($\langle D \rangle = 138$ nm), $\langle W \rangle_{mag}$ is similar to $\langle W \rangle_{nuc}$ (their ratio at low temperature is about 1.4), then for S1 ($\langle D \rangle = 100$ nm), the ratio $\langle W \rangle_{mag}/\langle W \rangle_{nuc}$ is about 4.5.

From the results of the Rietveld refinement, it is possible, in principle, to extract information about the microstructural characteristics of the species. As already mentioned, these would be averaged across all the peaks included in the analysis and, hence, possible anisotropic effects might be missed. Instead, we applied a more reliable and accurate procedure based on the independent determination of all the observed peak widths, and the analysis of their functional dependence on the d-spacings. The main steps of this procedure are discussed below.

3.2 Analysis of the diffraction peak widths

Earlier, it was shown for HRFD [28] that for a sample without strain and size effects (no microstrains, and large coherently scattering domains), the dependence of the peak width on the d-spacing is reproduced with good accuracy by the expression $(\Delta d_R)^2 = C_1 + C_2 \cdot d^2$, where C_1 and C_2 are linked in some way to the diffractometer parameters (flight path, chopper speed, beam collimation etc). Then, in the presence of a microstrain ε (static variance of metric parameters) in a coherent domain of finite size L, an additional broadening of diffraction peaks occurs. According to the Williamson–Hall analysis (for a state of the art review, see, e.g. Ref. [29]) the additional broadening $(\Delta d_\delta)^2$ associated with strain and size effects in the d-spacing scale can be expressed as $(\Delta d_\delta)^2 \approx (2\varepsilon d)^2 + (d^2/L)^2$ if a Gaussian approach for the distribution functions is used. Combining $(\Delta d_R)^2$ and $(\Delta d_\delta)^2$, we obtain the following expression for $(\Delta d)^2$ in terms of d^2:

$$(\Delta d)^2 = C_1 + (C_2 + C_3) \cdot d^2 + C_4 \cdot d^4, \qquad (1)$$

where $C_3 = (2\varepsilon)^2$ and $C_4 \approx (1/L)^2$ are free parameters, C_1 and C_2 are known from the resolution function. One can see that in the limit of very large crystallites, the dependence of $(\Delta d)^2$ on d^2 is linear, but is parabolic in the more general case. By employing this dependence over a sufficiently wide range of the measured d_{hkl}, it is possible to determine both ε and L. Since for NiO the overlapping of the nuclear and magnetic diffraction peaks is completely absent, it is possible to find ε and L independently for the nuclear and magnetic structures.

The diffraction peak widths (FWHM, full width at half-maximum) were found from the description of the peak profiles by the experimentally measured model function with the use of the UPEAK [30] program. When processing strongly overlapping peaks (weakly split due to rhombohedral lattice distortion), their positions were fixed in

Table 1 Structural data for NiO sub-micron powders obtained at $T = 5$ and 293 K. The conventional experimental (R_e) and weighted R-factors (R_ω) and χ^2-value, rhombohedral lattice parameters (a, α), cell volume (V), and oxygen thermal factor (B(O)) parameters are given. The average width of nuclear, $\langle W\rangle_{nuc}$, and magnetic, $\langle W\rangle_{mag}$, peaks (in arbitrary units) is also specified.

		sample		
parameter	T (K)	S3 (1500 nm)	S2 (138 nm)	S1(100 nm)
χ^2	293 / 5	4.7 / 4.7	5.0 / 4.3	3.0 / 2.5
R_ω	293 / 5	5.4 / 6.1	5.6 / 7.1	6.9 / 8.4
R_e	293 / 5	7.0 / 7.7	6.9 / 8.9	9.2 / 11.9
$\langle W\rangle_{nuc}$	293 / 5	10(2) / 11(2)	25(3) / 24(3)	60(4) / 55(4)
a (A)	293	2.9516(1)	2.9512(1)	2.9514(1)
	5	2.9466(1)	2.9465(1)	2.9462(1)
α (°)	293	60.073(1)	60.073(1)	60.064(1)
	5	60.090(1)	60.091(1)	60.090(1)
V (Å^3)	293 / 5	18.214 / 18.127	18.206 / 18.125	18.204 / 18.121
B(O) (Å^2)	293 / 5	0.12(1) / 0.1	0.29(1) / 0.1	0.17(1) / 0.1
$\langle W\rangle_{mag}$	293 / 5	12(3) / 12(3)	50(5) / 34(5)	219(10) / 252(10)

accordance with the Rietveld analysis. Additionally, for single peaks, the integral breadths were determined, i.e., the $W_{int} = S/A$ values, where S is the peak area and A is its amplitude. The results of these two approaches coincided with good accuracy; therefore, only the values obtained by the profile analysis are given and discussed below.

The analysis of Eq. (1) was performed using conventional method of least squares. In all the cases considered below, almost all experimental points are described by this function within statistical uncertainties, respectively the goodness of fit in each case was close to unity.

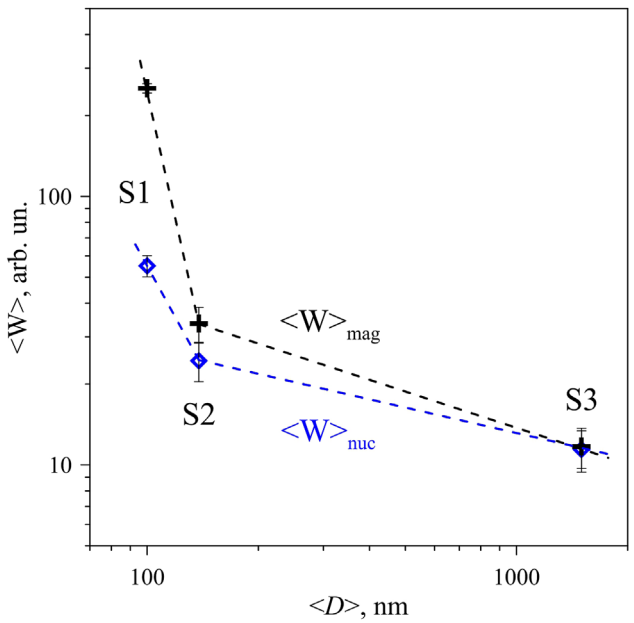

Figure 5 Dependences of average width of diffraction peaks of nuclear ($\langle W\rangle_{nuc}$, diamonds) and magnetic ($\langle W\rangle_{mag}$, crosses) phases on average particle size defined by Rietveld processing of low-temperature data for S1, S2, and S3 samples.

For sample S3 (1500 nm) the dependencies of $(\Delta d)^2$ on d^2 are linear for both the nuclear and magnetic peaks at room and low temperatures (Fig. 6), i.e., the size effect is absent. A slightly increased slope in comparison with the resolution function means the existence of a small level of microstresses identical for both (crystal and magnetic)

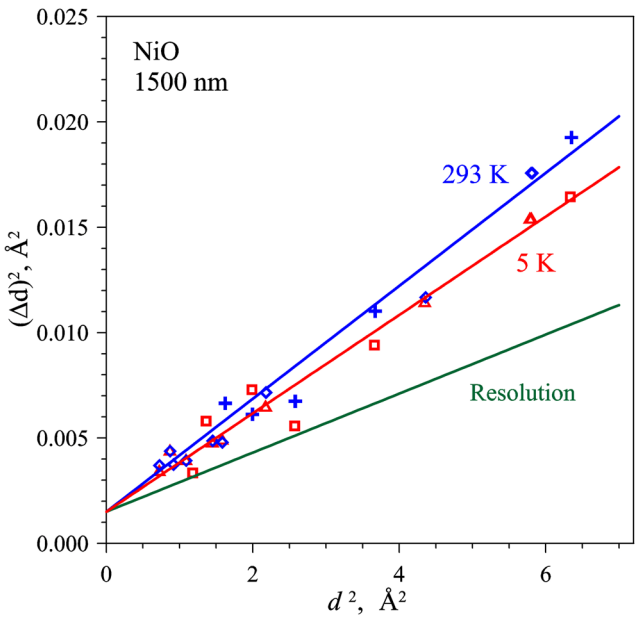

Figure 6 Dependences of diffraction peak widths on d-spacing for the S3 (1500 nm) sample. Experimental points are shown for crystal (diamonds and triangles) and magnetic (crosses and squares) phases and for two temperatures: 293 K (crosses and diamonds) and 5 K (squares and triangles). The dependences are linear, i.e., size effect is absent. The level of microstresses is smaller at lower temperature. Statistical errors of experimental points are about symbol size. Bottom line corresponds to the diffractometer resolution function measured with standard samples. The $(\Delta d)^2$ values are multiplied by 10^3.

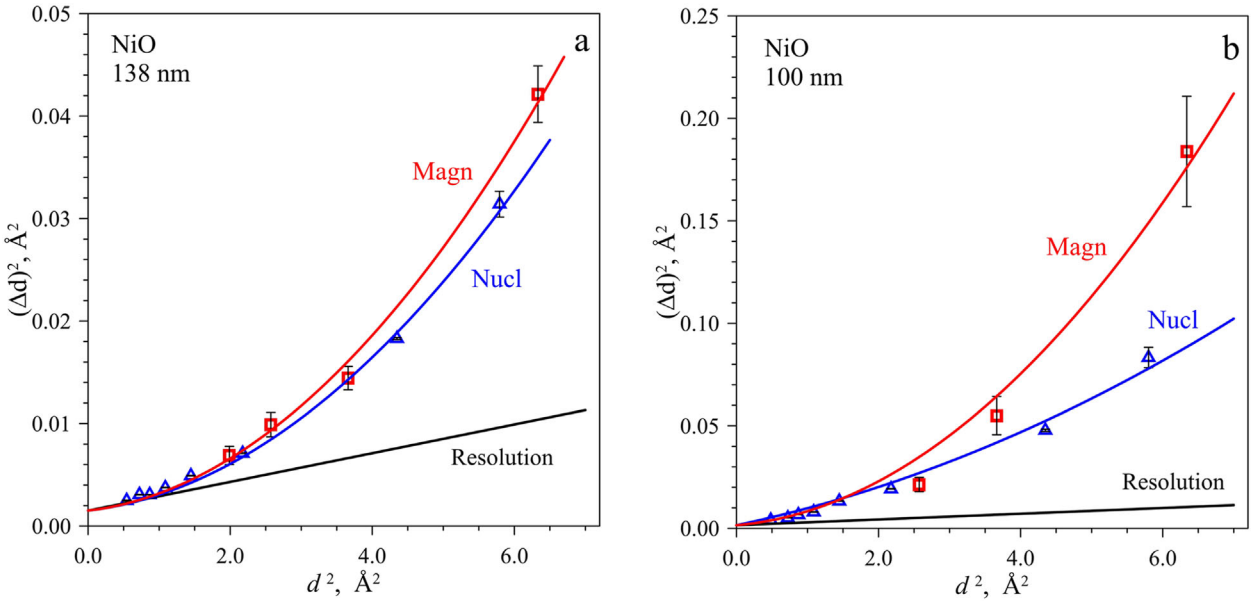

Figure 7 Dependences of diffraction peak widths on d-spacing for the S2 (a, 138 nm) and S1 (b, 100 nm) samples. Experimental points measured at 5 K are shown for crystal (triangles) and magnetic (squares) phases. Parabolic behavior is connected with the size effect. Resolution function measured with standard samples is also shown. The $(\Delta d)^2$ values are multiplied by 10^3.

phases, which slightly decreases (from $\varepsilon = 0.00057$ to 0.00048) with a lowering of the temperature.

In Fig. 7, similar dependencies for the submicron samples S2 (138 nm) and S1 (100 nm) are shown. They are both parabolic, which indicates that there is a size effect. It is remarkable that if for S2, the widths of the nuclear and magnetic peaks are close to each other and even can be described (within the statistical error bars) by the same parabola, for S1, two parabolas with rather different values of the C_4 coefficient are required.

The extraction of the coherently scattering domain sizes from the available peak width data was performed with several options, which yielded for 293 and 5 K slightly different sets of values of L_{nuc} and L_{mag}. After additional averaging, the final estimates of the nuclear and magnetic domain sizes are presented in Table 2, where the differences between the upper and lower limits are specified as uncertainties in brackets.

3.3 The Ni magnetic moment

In the Rietveld refinements, a magnetic structure was included in the simplest collinear option, assuming the AFM ordering of the Ni moments described in a preceding section. The values of the moments were refined by processing the high and average resolution diffraction patterns with the use of the FullProf program, which led, for both data sets, to almost identical numerical results.

The refined magnetic moments estimated for the different species are listed in Table 2. From these estimates, there is some slight trend (of about 5%) of the moment increase with decreasing grain size. However, the same points within their uncertanties correspond to the average value.

Table 2 The sizes of coherently scattering domains for crystal (L_{nuc}) and ordered magnetic (L_{mag}) phases, and the magnetic moment M_{Ni} of nickel atoms at room and low temperatures.

sample	S3 (1500 nm)	S2 (138 nm)	S1 (100 nm)
L_{nuc}, nm	$\gg$350	130(4)	78(4)
L_{mag}, nm	$\gg$350	118(4)	53(3)
M_{Ni}, μ_B (293 K)	1.91(4)	2.01(6)	1.94(7)
M_{Ni}, μ_B (5 K)	2.03(5)	2.18(6)	2.14(10)

4 Discussion

In the present study, high-resolution neutron diffraction measurements of three NiO powder samples clearly indicate that the crystalline structure and magnetic order inherent in the bulk material are still preserved inside fine NiO particles over a wide range of probed average sizes $\langle D \rangle$ of grain/particle, from bulk material ($\langle D \rangle = 1500$ nm) down to 100 nm. The results obtained for the average sizes of the crystalline and magnetic domains, L_{nuc} and L_{mag}, that scatter neutrons coherently are summarized and interpreted as follows.

In sample S3 ($\langle D \rangle = 1500$ nm), the obtained sizes of both the crystalline and magnetic domains obviously exceed 350 nm, which is the threshold limit for registration of size effects with HRFD. Thus, from the standpoint of diffraction, this sample can be regarded as a bulk one. For sample S2 ($\langle D \rangle = 138$ nm), the sizes of the crystalline and magnetic domains, estimated as $L_{nuc} \approx 130$ nm and $L_{mag} \approx 118$ nm, are somewhat less than the average grain size. Here, the observation that $L_{nuc} \sim \langle D \rangle$ indicates clearly that these

submicrometer grains are substantially single crystallites. Since the thickness of the magnetically disordered shell is larger than that of the structurally disordered one, $L_{nuc}/L_{mag} \approx 1.1$, we deduce that the magnetic order is suppressed in a larger fraction of the particle volume than the crystalline one is.

Because the surface-to-volume ratio increases inversely to the particle size, one expects that the effects of the surface disorder are further enhanced for smaller particles. This conjecture is supported by considering sample S1 ($\langle D \rangle = 100$ nm), where $L_{nuc} \approx 78$ nm and $L_{mag} \approx 53$ nm are, again, to be regarded as the characteristics of the core. Therefore, the two relative fractions of the particle volume, which we attribute either to the structurally disordered or magnetically disordered shell, are considerably larger than those in sample S2. Moreover, for the smaller particles in the S1 sample, i.e., on the boarder of the nanorange (<100 nm), one has $L_{nuc}/L_{mag} = 1.5$, which means that an increase of the surface-to-volume ratio has a progressively stronger effect on the magnetism in the submicron AFM particles. This conclusion is independently corroborated by the relationship between the peak width parameters obtained after Rietveld refinement as well.

The nature of near-surface disordered shell is not known, but the most obvious reason is that a near-surface region of NiO is less stoichiometric than the core. Actually, a typical bulk nickel oxide is a p-type semiconductor whose properties are strongly influenced by native defects including the dominant Ni vacancies, together with some minor admixure of Ni interstitials and/or oxygen vacancies/interstitials. It is expected that the defect formation energies in the near-surface region are considerably different compared to the bulk ones due to various uncompensated effects on the surface, and these effects provoking the defect formation enhance with an increase of the surface-to-volume ratio [15]. Depending on a preparation procedure of NiO particles, the defect density may exceed a critical value, which leads to some reconstruction or amorphization of the near-surface region of a particle.

Concerning the issue of the defect distribution over the particle volume, we suggest that their concentration decreases with depth below the outer subshell such that the regular lattice structure is gradually restored inside the particle. Even so, in the intermediate region, where the typical structural order is at least partially restored and contributes to the measured L_{nuc}, i.e., in the submerged subshell below the outer one, but above the core, the dominant Ni-vacancy defect concentration is still high enough to destroy the magnetic ordering (see Ref. [15], where the core–shell model of the vacancy concenration in NiO fine particles from the nano- to the submicron size is developed). Actually, the nickel vacancy produces, first, a local magnetic moment located on oxygens around the vacancy and, second, a local change of electronic structure, which introduces a few holes propagating in the the surrounding region of the anionic sublattice. As a result, the ferromagnetic coupling between the moments of the host nickel sublattice appears due to the double exchange that competes with the antiferromagnetic superexchange inherent to the regular stoichiometric NiO. These competing interactions and randomness of vacancy sites enhance magnetic disorder and make the submerged subshell to behave as a spin glass.

Although the present neutron diffraction measurements provide strong evidences in favor of the core–shell model of the vacancy concentration, which is only slightly generalized to involve into consideration the fully disordered outermost subshell, a more detailed and precise characterization of the lattice and magnetic structure on the atomic scale in the shell region cannot be obtained with the use of the applied method only. Certainly, complementary surface sensitive techniques, for instance, EXAFS and XANES (as it has been realized in Ref. [15]), have to be applied to help a better understanding of the entire system.

We should make a remark concerning the shape of NiO particles under considerations. As already noted (see, e.g., Refs. [20, 21]), nanosized NiO particles may have, for instance, a disc-like shape with a diameter exceeding many times its thickness. Assuming such a shape, we should observe an anisotropic broadening of the diffraction peaks (both nuclear and magnetic), i.e., a correlation between the width and a particular set of Miller indices (see, e.g., [31]). However, in the quadratic dependencies of $(\Delta d)^2$ on d^2 that were derived (Fig. 7), no such anisotropic effects are seen and, in particular, there is no correlation between the size of the coherent domain and the orientation of its crystallographic axes.

According to the neutron diffraction data available in the literature [32, 33], the measured magnetic moment of the nickel atom regarded as the bulk value in NiO is $M_{Ni} = 1.90(6)\mu_B - 2.02(4)\mu_B$ (at $T = 2$–5 K), which is close to the spin-only value $2\mu_B$ for Ni^{2+}. In fact, the orbital moment of the valence electrons of nickel atoms in NiO is not fully quenched, and the reported value of M_{Ni} is due to a subtle balance between the reduced spin moment and the orbital one [34, 35]. From our measurements, the size-averaged value of the nickel magnetic moment for each of samples S1–S3 was found to be $(1.96 \pm 0.03)\mu_B$ at room temperature and $(2.12 \pm 0.03)\mu_B$ at low temperatures. Each of these values is independent, within the experimental uncertainties, of the size of the grains, and both are close to those reported in Refs. [32, 33].

5 Conclusions The crystal structure and magnetic order have been studied by neutron diffraction in fine particle NiO powders with grain sizes, estimated by the Brunauer–Emmett–Teller method, ranging from 100 to 1500 nm. An accurate analysis of high resolution TOF neutron diffraction patterns containing many nuclear and several magnetic lines allowed us to separate the contributions of the coherently scattering structural (nuclear) and magnetic domains and measure their characteristic lengths, L_{nuc} and L_{mag}, respectively (Table 2). Within these domains, the presence of the antiferromagnetic order

at and below room temperature, and the related rhombohedral distortion of the crystal lattice inherent to the bulk NiO, has been confirmed in all samples.

For two poweder samples whose mean particle sizes $\langle D \rangle$ are on the border of the nanorange, it was found by both Rietveld and Williamson–Hall methods, first, that $L_{mag} < L_{nuc} \leq \langle D \rangle$, which suggests the presence of the ordered core part of a particle and a shell that is disordered due to surface effects, and, second, the ratio L_{nuc}/L_{mag} increases for smaller $\langle D \rangle$, thus indicating more rapid degradation of long range magnetic order, in comparison with the atomic one, with decreasing particle size. We use the $L_{nuc} \leq \langle D \rangle$ relationship between sizes of particles and coherently scattering atomic domains because of uncertainty on $\langle D \rangle$ determined by the BET method could be quite large. These observations should be considered as a sort of finite-size effects that has to be interpreted in terms of the core–shell model of the vacancy concentration in NiO particles of submicron size. Verification of this picture requires further work with the use of other experimental techniques for a better characterization of the particle surface.

Acknowledgements The experiments at the IBR-2 reactor were performed within the proposals nos. 2013-10-31-17-50-26 and 2014-04-16-13-41-23. This work was supported by RFBR (the Russian Foundation for Basic Research) 14-29-04091_ofi_m and partially (A.K. and N.M.-U.) by the Latvian Science Council grant no. 187/2012.

References

[1] X. Batlle and A. Labarta, J. Phys. D, Appl. Phys. **35**, R15 (2002).
[2] R. Skomski, J. Phys.: Condens. Matter **15**, R841 (2003).
[3] M. R. Fitzsimmons, S. D. Bader, J. A. Borchers, G. P. Felcher, J. K. Furdyna, A. Hoffmann, J. B. Kortright, I. K. Schuller, T. C. Schulthess, S. K. Sinha, M. F. Toney, D. Weller, and S. Wolf, J. Magn. Magn. Mater. **271**, 103 (2004).
[4] S. P. Gubin, Y. A. Koksharov, G. B. Khomutov, and G. Y. Yurkov, Russ. Chem. Rev. **74**, 489 (2005).
[5] B. Barbara, Solid State Sci. **7**, 668 (2005).
[6] G. Srajer, L. H. Lewis, S. D. Bader, A. J. Epstein, C. S. Fadley, E. E. Fullerton, A. Hoffmann, J. B. Kortright, K. M. Krishnan, S. A. Majetich, T. S. Rahman, C. A. Ross, M. B. Salamon, I. K. Schuller, T. C. Schulthess, and J. Z. Sun, J. Magn. Magn. Mater. **307**, 1 (2006).
[7] S. Mørup, D. E. Madsen, C. Frandsen, C. R. H. Bahl, and M. F. Hansen, J. Phys.: Condens. Matter **19**, 213202 (2007).
[8] F. J. Himpsel, J. E. Ortega, G. J. Mankey, and R. F. Willis, Adv. Phys. **47**, 511 (1998).
[9] A. Hernando, J. Phys.: Condens. Matter **11**, 9455 (1999).
[10] K. Bennemann, J. Phys.: Condens. Matter **22**, 243201 (2010).
[11] A. Anspoks, A. Kalinko, R. Kalendarev, and A. Kuzmin, Phys. Rev. B **86**, 174114 (2012).
[12] L. Li, L. Chen, R. Qihe, and G. Li, Appl. Phys. Lett. **89**, 134102 (2006).
[13] S. A. Makhlouf, M. A. Kassem, and M. A. Abdel-Rahim, J. Mater. Sci. **44**, 3438 (2009).
[14] W. J. Duan, S. H. Lu, Z. L. Wu, and Y. S. Wang, J. Phys. Chem. C **116**, 26043 (2012).
[15] S. Mandal, S. Banerjee, and K. S. R. Menon, Phys. Rev. B **80**, 214420 (2009).
[16] E. Winkler, R. D. Zysler, M. V. Mansilla, D. Fiorani, D. Rinaldi, M. Vasilakaki, and K. N. Trohidou, Nanotechnology **19**, 185702 (2008).
[17] S. Tiwari and K. Rajeev, Thin Solid Films **505**, 113 (2006).
[18] N. Rinaldi-Montes, P. Gorria, D. Martínez-Blanco, A. B. Fuertes, L. Fernández Barquín, J. Rodríguez-Fernandez, I. de Pedro, M. L. Fdez-Gubieda, J. Alonso, L. Olivi, G. Aquilanti, and J. A. Blanco, Nanoscale **6**, 457 (2014).
[19] M. P. Proenca, C. T. Sousa, A. M. Pereira, P. B. Tavares, J. Ventura, M. Vazquez, and J. P. Araujo, Phys. Chem. Chem. Phys. **13**, 9561 (2011).
[20] J. F. K. Cooper, A. Ionescu, R. M. Langford, K. R. A. Ziebeck, C. H. W. Barnes, R. Gruar, C. Tighe, J. A. Darr, N. T. K. Thanh, and B. Ouladdiaf, J. Appl. Phys. **114**, 083906 (2013).
[21] S. Klausen, P.-A. Lindgård, K. Lefmann, F. Bødker, and S. Mørup, Phys. Status Solidi A **189**, 1039 (2002).
[22] N. Mironova-Ulmane, A. Kuzmin, J. Grabis, I. Sildos, V. I. Voronin, I. F. Berger, and V. Kazantsev, Solid State Phenom. **168–169**, 341 (2011).
[23] A. M. Balagurov, I. A. Bobrikov, J. Grabis, D. Jakovlevs, A. Kuzmin, M. Maiorov, and N. Mironova-Ulmane, IOP Conf. Ser.: Mater. Sci. Eng. **49**, 012021 (2013).
[24] N. Mironova-Ulmane, A. Kuzmin, I. Steins, J. Grabis, I. Sildos, and M. Pärs, J. Phys.: Conf. Ser. **93**, 012039 (2007).
[25] A. M. Balagurov, Neutron News **16**, 8 (2005).
[26] V. Zlokazov and V. Chernyshev, J. Appl. Crystallogr. **25**, 447 (1992).
[27] J. Rodríguez-Carvajal, Physica B **192**, 55 (1993).
[28] A. Balagurov, V. Pomjakushin, V. Simkin, and A. Zakharov, Physica C **272**, 277 (1996).
[29] E. J. Mittemeijer and U. Welzel, Z. Kristallogr. **192**, 55 (1993).
[30] V. Zlokazov, Nucl. Instrum. Methods **130**, 543 (1975).
[31] V. Kazimirov, M. Smirnov, L. Bourgeois, L. Guerlou-Demourgues, L. Servant, A. Balagurov, I. Natkaniec, N. Khasanova, and E. Antipov, Solid State Ionics **181**, 1764 (2010).
[32] E. Brok, K. Lefmann, P. P. Deen, B. Lebech, H. Jacobsen, G. J. Nilsen, L. Keller, and C. Frandsen, Phys. Rev. B **91**, 014431 (2015).
[33] A. K. Cheetham and D. A. O. Hope, Phys. Rev. B **27**, 6964 (1983).
[34] S. K. Kwon and B. I. Min, Phys. Rev. B **62**, 73 (2000).
[35] W. Jauch and M. Reehuis, Phys. Rev. B **70**, 195121 (2004).

